DJS Vol. 49 (1) (2024) – pp. 131-151 ISSN: 1012-5965

Delta Journal of Science
Available online at
https://djs.journals.ekb.eg/

Research Article

GEOLOGY

Studying the Effect of Saltwater Intrusion on the Quaternary Aquifer Using Geophysical techniques, El Amal City, East Ismaillia, Egypt

Ahmed Nasr *

Geophysical Exploration Department, Desert Research Center, Cairo, Egypt.

*Corresponding author: Ahmed Nasr *e-mail*: dr_a_nasr86@yahoo.com

Received: 8/10/2024 **Accepted:** 21/10/2024

KEY WORDS

Seawater intrusion.

Groundwater.

Geophysics.

Coastal aquifers.

ABSTRACT

This study aims to identify horizontal and vertical brackish water zones within the quaternary aquifer of a resource-rich area using a combination of hydrochemical and geophysical methods. Fourteen groundwater and two surface water samples were analyzed for major anions and cations to assess water quality and saltwater intrusion. The seawater mixing index, based on concentrations of magnesium, sodium, sulfate, and chloride ions, was calculated to estimate seawater intrusion. Additionally, a groundwater quality index was developed to quantify the degree of seawater intrusion. Sixteen Schlumberger Vertical Electrical Soundings and ten 2D profiles were conducted along two lines, revealing four geoelectrical layers: dry fine sand and silt, brackish water-bearing sand and silt, saline water-bearing sand and silt, and clay. Layers B and C contain water, and the findings indicate that groundwater near the Suez Canal shows signs of saltwater intrusion. However, 50% of samples also suggest dissolution of marine deposits or freshwater. The study recommends drilling new wells up to 76 meters deep in the eastern part of the area, while hand-dug wells are suitable for the western region at depths of 8 meters.

Introduction

The coastal aquifer is vulnerable to infiltration by seawater as a result of excessive extraction of groundwater **(Tomaszkiewicz et al., 2014)**. Saltwater intrusion significantly degrades the quality of groundwater. Consequently, brackish water serves as an interface between fresh and saltwater, with the denser saltwater carrying the less dense water **(Bear, 1999)**. On the contrary, the release of significant quantities of fresh groundwater from aquifers along the coast leads to a decrease in the pressure of the fresh water, stimulating an additional movement of the ocean towards land. The infiltration of seawater into a coastal aquifer occurs due to the pumping of groundwater from the aquifer. As a result, the freshwater level decreases. **Qahman et al. (2005)** states that a multitude of natural and/or anthropogenic limitations influence the water quality in coastal aquifers. **Appelo and Postma (2005), Panteleit et al. (2011)** and **Boluda-Botella et al. (2014)** have proven that water-rock interaction processes and the mixing of distinct water sources (freshwater and saltwater) affect the chemical composition of coastal groundwater. In order to ensure the integrity of coastal groundwater, a comprehensive understanding of the systems that regulate the movement of saltwater is required **(Gibbs et al., 2013)**. As a result, conducting research on seawater infiltration into coastal aquifers is critical for identifying affected zones and facilitating the development of appropriate remediation strategies or preventative measures. An integrative strategy was employed to examine seawater intrusion by utilizing a mix of hydrochemical and geophysical techniques **(Kouzana et al., 2010; Najib et al., 2017)**. This study uses the modified Hydrochmical Faces Evaluation Diagram (HFED), the Saltwater Mixing Index (SMI), and the Ground Water Quality Index (GWQI) to look at how seawater gets into coastal aquifers. Researchers have successfully identified the interface between freshwater and saltwater in coastal aquifers using geophysical techniques, specifically geoelectric approaches **(Barker, 1980)**. A DC resistivity approach is among these techniques. Aquifer resistivity decreases in regions with substantially saline groundwater. Consequently, the resistivity approach can delineate the limits of saline water bodies **(Hassan et al., 2019; Qudsiah et al., 2024)**. **Griffith and Barker (1993)** highlight the significant difference in resistivity at the freshwater-saltwater boundary when sharing the results of

their resistivity survey. Furthermore, the identification of saltwater intrusion in diverse coastal areas has been made possible by a number of researchers by the substantial differences in resistivity between zones saturated with freshwater and saltwater **(Frohlich et al., 1994; Kusumayudha et al., 2023)**. The study's objectives are to find sources of freshwater and saltwater, describe the hydrochemical changes in the coastal aquifer using both hydrochemical and geophysical methods, find the vertical and horizontal brackish water zones in the Eastern Suez Canal Region of Egypt, and suggest places to drill groundwater wells to ensure safe groundwater withdrawal.

The Geologic Overview

The study area is in the eastern part of the Suez Canal on the Sinai Peninsula. This area covers approximately 50 km2 and lies between latitude 30.69 to 30.72N and longitude 32.37 to 32.42E (Fig. 1). The local Mediterranean climate affects the area under investigation. The rainfall average ranges from 41 to 50 mm/year and increases from southeast to northwest **(Elewa and Qaddah, 2011).**

El Abd, (2000) records a minimum air temperature of 13.7°C during the winter and a maximum of 29°C during the summer, with a relative humidity ranging from 53.5°C to 60%. Geomorphologically, the surface elevation varies from +2 m in the west to +76 m above sea level (a.s.l.) in the eastern stretches. Wind activity dominates the northwestern portion of Sinai, influencing the geomorphological features **(Diab, 1998).** Two distinct geomorphic units, characterized by low inland dunes, sand hummocks, salt marshes, and sabkhas, divide the area. Geological separation of the Quaternary sediments occurred between the Holocene and Pleistocene periods. During the Holocene, two formations occurred: Sabkha, situated in the northwestern region of the research area along the eastern bank of the Suez Canal, is the initial structure identified. Because of the presence of sand dunes and sand sheets, the second formation covers the majority of the area under investigation. Representative of the Pleistocene deposits, the Al Qantara Formation primarily consists of sand and gravel, with trace amounts of clay interbedded **(Sultan et al., 2009).** During the Middle Miocene, the stratigraphic sequences consisted of alluvium deposits, which reached depths of 30 to 80 meters and were up to 30 meters deep. These deposits are composed of sandy clay. Two formations characterize the Lower-Middle Miocene: the initial formation comprises mud and clay at depths between 80 and 230 meters, while the subsequent formation consists of

sandstone and clay. Figure (2) shows that the Miocene layers are on top of the Lower Cretaceous, which is made up of clay-intercalated sandstone and shows the deep Nubian sandstone aquifer in the area. The Quaternary aquifer is the primary shallow aquifer within the investigated region. The lithology of the aquifer consists of interbedded sand, silt, and clay. The direction of groundwater flow is northwest **(Sultan et al., 2009).** The salinity of the water increases in response to groundwater movement. Irrigation canals and their tributaries supply freshwater to this region, directly recharging the water and resulting in low salinity. The water table rises or falls by 28.2 meters. The aquifer's thickness is between 40 and 52 meters. The aquifer's transmissivity is roughly 300 m^2/day. **Sultan et al., (2009)** estimates the aquifer recharge to be around 40,000 m^3/day, while the overall abstraction is 10,000 m^3/day.

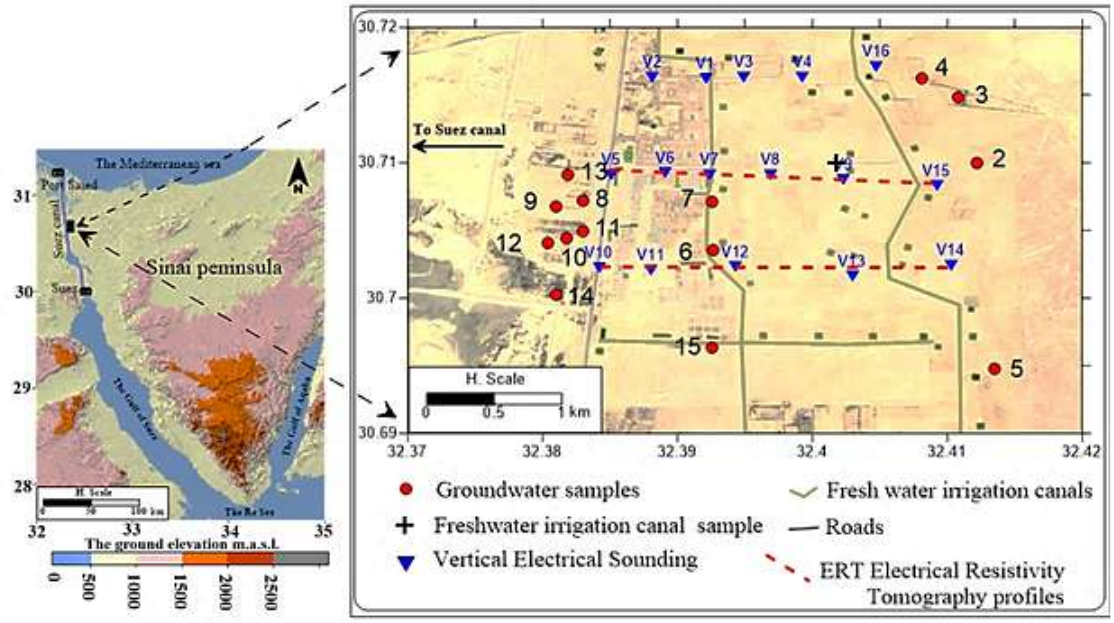

Fig. (1): The location map of the study area

Materials and Methods

Geoelectrical Measurements

Geophysical surveying is a suitable technique for detecting the impacts of subterranean structures on coastal regions, as well as for studying, assessing, and mapping groundwater supplies. This study has the potential to be utilized in the selection of optimal locations for risk-free well design and production. To achieve the study's objective, we conducted a series of sixteen VESes and ten 2D imaging profiles along two lines oriented in the west-east direction. The VES measurements were conducted utilizing a Schlumberger electrode array in which the separation between the AB current electrodes did not exceed one thousand meters. The employed electrode

separation was sufficient to attain a rational depth range, thereby fulfilling the research objective. A geoelectrical interpretation that was parameterized and calibrated involved the execution of one of the soundings adjacent to a borehole. In consideration of the overall configuration of the sounding curves, an arbitrary beginning model has been built. For the quantitative analysis of the geoelectric sounding curves, the RESIST computer software and IPi2 Win v.2.1, 2003, were utilized **(Abdel Hafeez et al., 2018)**. The application implements a layered earth model, a graphical modelling tool, enabling users to evaluate resistivity curves. The software provides support for both forward and inverse modelling methods, in addition to interactive functionalities that enhance the user experience. The 2D resistivity image obtained using the more conventional VES method provides complementary supply information **(Zayed and Nasr, 2023).** Therefore, it can be used for both hydrogeological and engineering purposes **(Al-Mahemmdi et al., 2023).** Utilizing the multi-electrode resistivity approach, 2D resistivity imaging was performed along two lines (Figs. 1 and 3). Wenner arrays were deployed over the whole length of each line, which spanned around 2.6 km. In order to determine resistivity using the multi-electrode method, a multi-core wire comprised of 39 conductors, each functioning as an electrode is utilized. These conductors are put into the ground at consistent intervals of five meters. At various electrode spacings, the "ABEM Terameter SAS 1000" resistivity meter (Fig. 4) is utilized to provide precise geoelectrical readings. Once the series of measurements is complete, the program performs an automatic verification of the electrode contact and then scans in accordance with a pre-established measurement routine. The examination of the resistivity data in two dimensions was performed utilizing version 3.4 of the RES2DINV computer software **(Loke, 1999).**

Water Sampling and Hydrochemical Analysis

For the groundwater quality assessment, fourteen groundwater and two surface water samples were collected during August 2020 (Fig. 1). The two surface water samples represent the freshwater irrigation canal and Suez Canal water. As per **Brown et al. (1983); Barer et al. (2000),** and **ASTM (2002)** (Table 1), water samples were taken and tested for Ca^{2+}, Mg^{2+}, Na^{+}, K^{+}, CO_3^{2-}, HCO_3^{-}, Cl^{-}, and SO_4^{2-}. The hydrogeochemistry laboratory at the Desert Research Centre (DRC), Cairo, Egypt, conducted the water analysis. Electrical conductivity (EC), pH, carbonate, and bicarbonate were measured in situ. The water

sample's locations were recorded using a Global Positioning System (GPS) receiver (model Garmin Etrex, Vista, HC). The chemical analysis quality was inspected using the electrical balance (E.B.%) **(Appelo and Postma, 2005)** as follows:

E.B% = [(∑total cations – ∑ total anions) / (∑total cations – ∑total anions)] × 100. The acceptable range of water quality assurance (E.B.) is within ±2%.

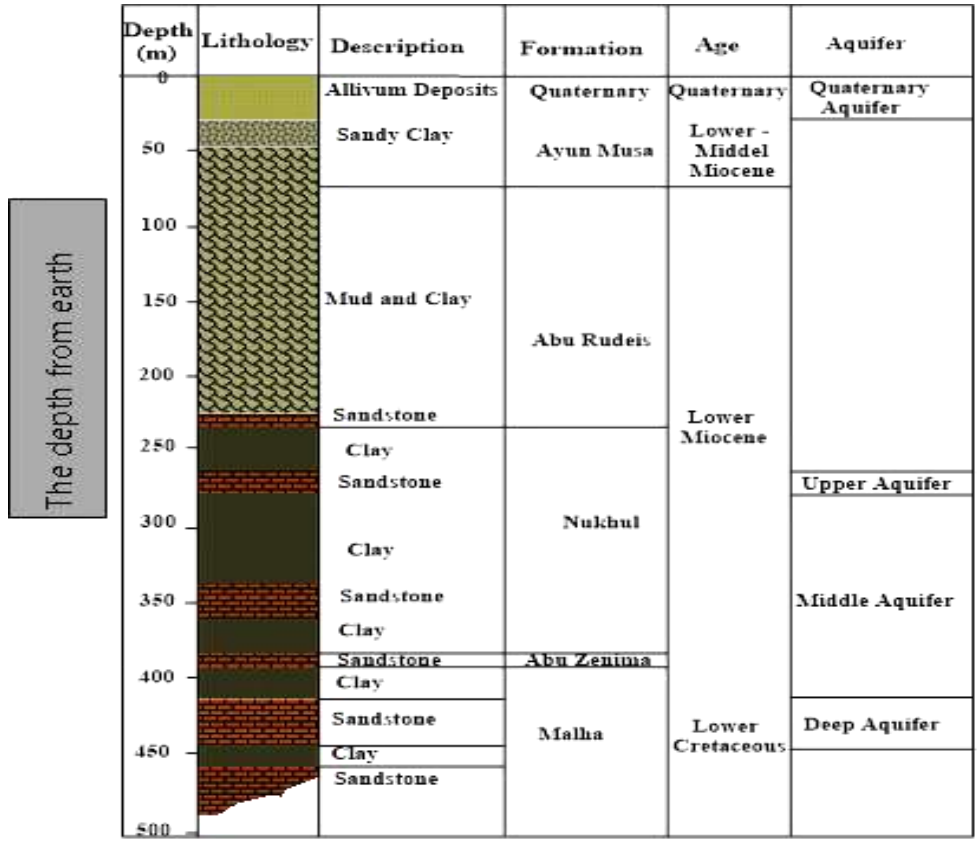

Fig. (2): Al Qantara borehole, at distance of 60 km south the study area at Ayun Musa Coast Village at latitude of 29° 50′ 31″ and longitude 32° 39′ 36″ of depth 500 m (Sultan et al., 2009).

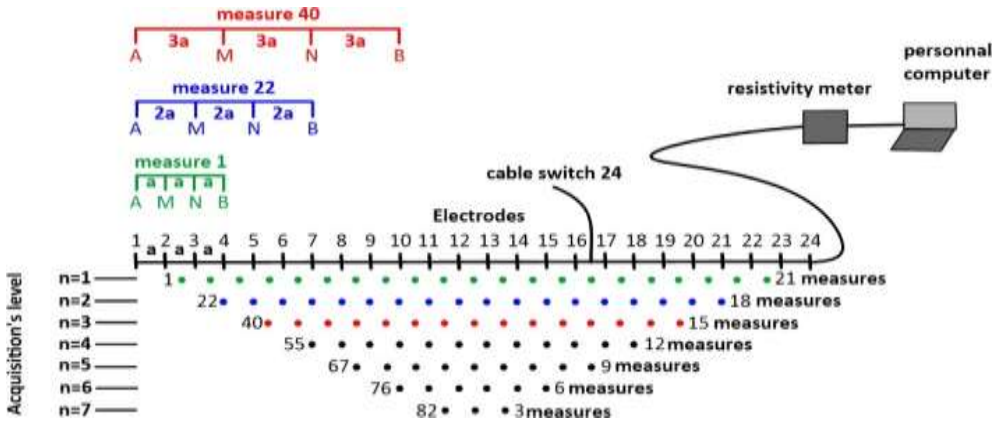

Fig. (3): Sequence of measurements to build up a pseudo section (After Clement et al., 2020)

Fig. (4): The instrument SAS 1000 with multi-electrode system and field photo.

Table (1): Instrumental/chemical methods used for water samples analysis**.**

Chemical constituent	Instrumental/chemical analysis methods
EC	Conductivity meter with selective electrode (Model: Greisinger GLF 100 RW)
pH	pH meter with selective electrode (Model: HANNA HI8424)
TDS	The summation total ionic counts (TDS = Ca^{2+}+ Mg^{2+} + Na^{+}+ K^{+}+ CO_3^{2-}+ HCO_3^{-2} + Cl^{-}+ SO_4^{2-})
Ca^{2+}, Mg^{2+}	Using inductive coupled plasma mass spectrometry (ICP, POEMSIII, thermo Jarrell elemental company USA).
Na^{+}, K^{+}	Flame photometer model PFP 7, Jenway, (UK)
CO_3^{2-}, HCO_3^{-}	Titrimetrically against sulphuric acid (0.01N) by neutralization method using phenolphthalein and methyl orange as indicators
Cl^{-}	Titrimetrically against $AgNO_3$ (0.014) using potassium chromate indicator.
SO_4^{2-}	Turbidity method using spectrophotometer (Model: PG, T60)

Hydrochemical Methods

The physiochemical information (Table 1) illustrates the process by which seawater infiltrates the coastal aquifer under investigation. The HFED **(Gime´nez-Forcada, 2010)** illustrates the temporal evolution of hydrochemical facies. It is utilized to locate the coastal aquifer during recharge and intrusion episodes. Piper diagrams and other typical diagrams are inadequate for illustrating the progression of groundwater facies changes that occur during intrusion and recharge phenomena. The HFED graphic provides greater clarity regarding the sequence of facies evolution. The HFED explained the primary ion concentrations in the groundwater chemistry process associated with the seawater intrusion interface: Ca^{2+}, Na^{+}, HCO^{3-}, SO_4^{2-}, and Cl^{-}. The HFED diagram will generate a mixing line, symbolizing the mixture of freshwater and saltwater. Seawater mixing index (SMI): **Mondal and Singh, (2011)** estimates the relative degree of mixing in specific waters using the following Mg^{2+}, Na^{+}, SO_4^{2-}, and Cl^{-} ion

concentrations: SWMI is calculated as follows:

[a (CNa/TNa)] + [b (CMg/TMg)] + [c (CCl/TCl)] + [d (CSO4/TSO4)]) (1)

In the given context, the constants a, b, c, and d represent the relative concentrations of Na^+, Mg^{2+}, Cl^-, and SO_4^{2-}, respectively (a = 0.31, b = 0.04; c = 0.57; d = 0.08). The concentration of groundwater samples is denoted as C, expressed in mg/l. Cumulative probability curve analysis establishes the regional threshold values of ions in groundwater samples, denoted as T. When the SMI value is computed to be more than one, it can be concluded that the water is evidently reflecting the impact of seawater mixing **(Park et al., 2005).** Groundwater quality index for seawater intrusion: In their study, **Tomaszkiewicz et al., (2014)** formulated the particular index to saltwater intrusion for groundwater samples (GQISWI) in the following manner:

GQISWI = [GQI Piper mix - GQI fsea] / 2 (2)

GQI Piper mix = [(Ca^{2+} + Mg^{2+} / Total cations)] + (HCO^{3-} / Total anions)] × 50 (3)

GQI fsea = (1 – fsea) × 100) (4)

fsea = [m Cl (sample) – m Cl (seawater)] / [m Cl (sample) – m Cl (fresh water)] (5)

Where GQISWI ranges from: 75–100 freshwaters; 50–75 mixed groundwater; 10–50 saline groundwater; and 0–10 sea waters.

Results and Discussion

Integrating interpreted measured geoelectrical data with the chemical analysis of water samples allowed this study to achieve its goal. The analysis of the acquired outcomes is presented as follows:

Geoelectrical Measurements

The survey of geoelectrical resistivity was performed utilizing standard 1D and 2D methodologies. The 1D VES survey determines the vertical and horizontal organization of the sedimentary sequence, the depth of the aquifer layers, and the demarcation between brackish and saline water. The methodology of two-dimensional electrical imaging (2D) depicts the spatial arrangement of electrical characteristics of subsurface strata within an uninterrupted image. This technique effectively captures data in both the horizontal and vertical planes. The findings of these geoelectrical approaches are succinctly described as follows:

The Vertical Electrical Sounding

The soundings' field data has been analyzed both qualitatively and quantitatively to accurately define the underlying sequence geological context in the study area, as outlined below:

To begin the qualitative interpretation, one must examine the interrelationships between the apparent resistivities, and thicknesses of the various strata depicted on the sounding curves (Fig. 5). This gives information concerning the number of layers, their uniformity or diversity within each layer, and their consistency across the region or in a certain direction. Two sorts of field curves can be distinguished: KQQ-types and KHKQ-types, according to a common characteristic. Nevertheless, despite variations in the layers' thicknesses (or depths), the apparent resistivity remains the same. The KHKQ and KQQ curve types are indicative of a geoelectrical layer categorization ranging from five to six. The clay or moist surface layer (surface water) is symbolized by the KH cycle, while the KQ cycle signifies the progression from dry gravel or sand to brackish water-bearing sand to saline water-bearing sand or clay. The geological data indicates that the subsurface succession in the region under investigation consists of alternating strata of sand, gravel, silt, sabkha, and clay.

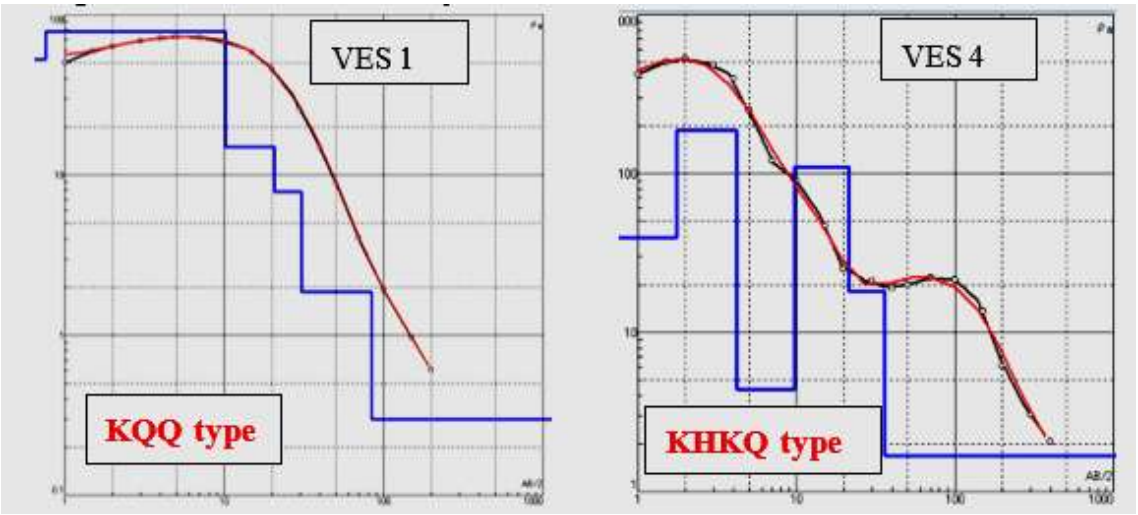

Fig. (5): Examples of the resistivity sounding curves in the study area (VESs No.1 and 4)

Quantitatively, a quantitative investigation was subsequently performed in order to build a multi-layer model that accurately represented the resistivity and thickness. By correlating precise resistivity measurements with lithological information gleaned from adjacent wells, geological data is utilized. Figure (6) illustrates the interpretation of the modelled resistivity sounding. VES initial number 1 using a series of geoelectrical cross sections-oriented west-east, the overall geological background and essential information regarding the composition of water-retaining rocks and strata are illustrated and documented. The examination of the field curves revealed that the four

principal strata denoted in Table 2 (A, B, C, and D) comprise the geoelectrical succession. Figure (1) depicts the geoelectrical cross sections in their respective places.

Table (2): The results of the quantitative interpretation of the geoelectrical field curves

Layer No.	Resistivity (Ohm.m)	Thickness (m)	Corresponding Lithology
A	>50	4 – 33	Dry fine sand and silt
B	10 - 20	4 - 40	Fine sand and silt (Brackish water-bearing)
C	5 - 10	6 - 33	Fine sand and silt (Saline water-bearing)
D	<5	--	Clay

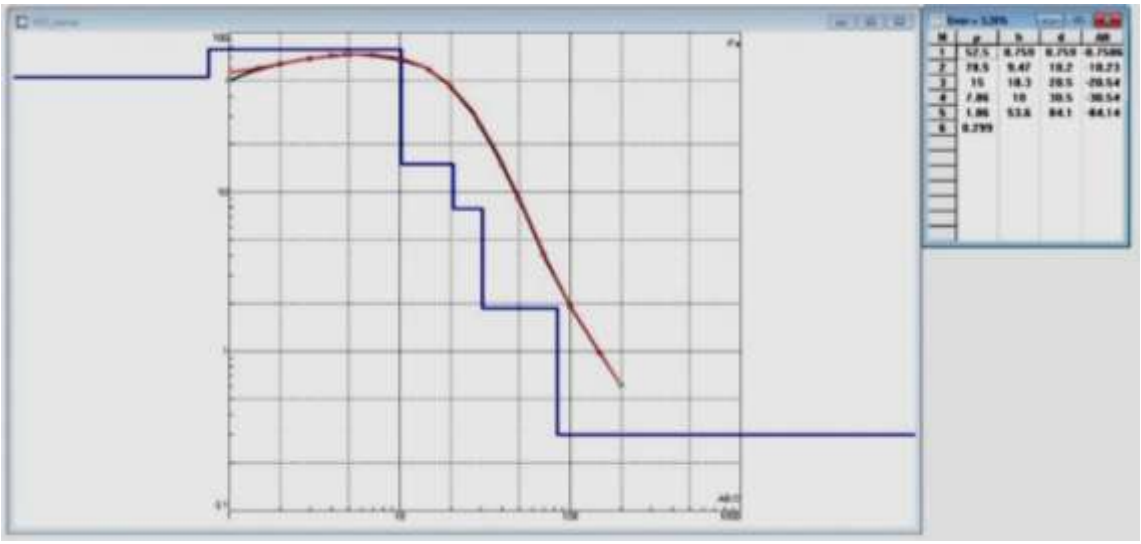

Fig. (6): Shows the interpretation of the modeled resistivity sounding VES No. (1)

Using VES geoelectrical properties, three cross sections (AA', BB', and CC') were generated, as shown in Figs. (7, 8, and 9) respectively. Each cross section is described from top to bottom: The uppermost layer (A) consists of dry fine sand, gravel, and silt with a resistivity over 50 Ohm.m, ranging from 4 to 33 meters thick. The second layer (B) indicates brackish water saturation with resistivity values of 10-20 Ohm.m, spanning 4-40 meters. Layer (C) comprises fine sand, gravel, silt, and clay, representing seawater saturation with a resistivity of 5-10 Ohm.m and a thickness of 6-33 meters. Layer (D) below 5 Ohm.m represents sabkha and clay sediments. The bottom boundary of this zone was not detected during soundings.

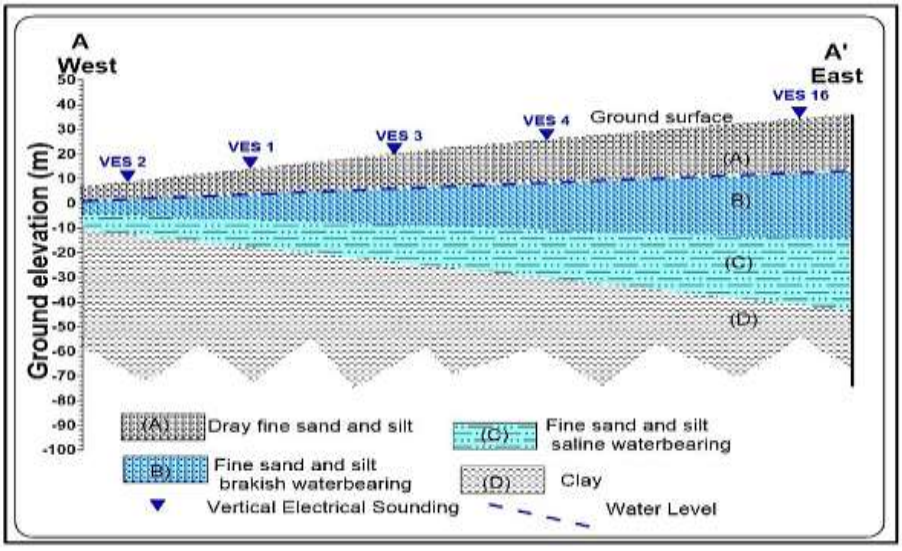

Fig. (7): Geoelectrical cross section A-A'

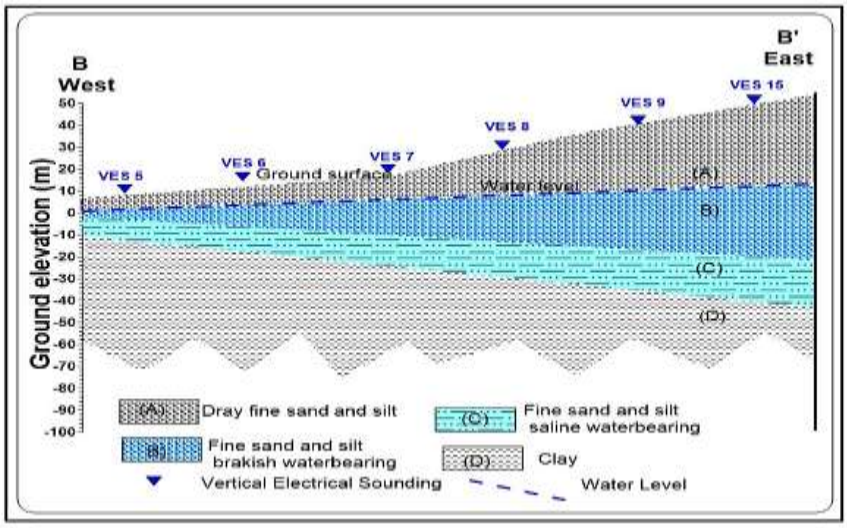

Fig. (8): Geoelectrical cross section B-B'

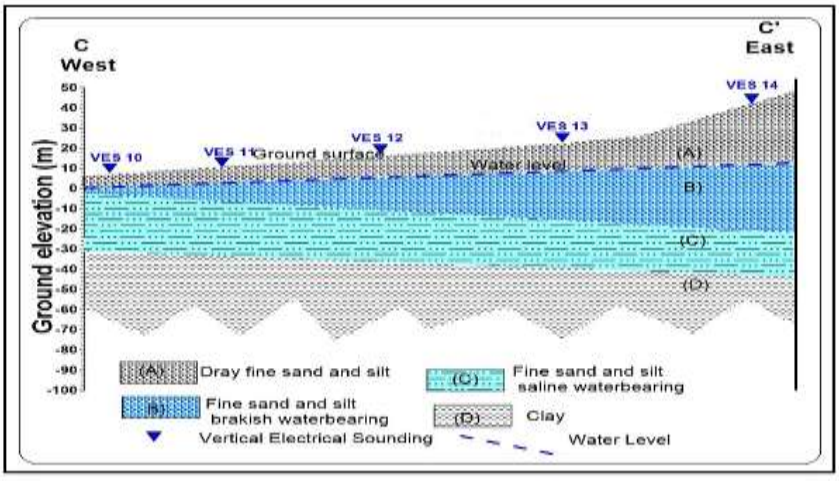

Fig. (9): Geoelectrical cross section C-C'

The 2D Imaging with Roll Along Configuration

Three profiles measured in a single direction comprise each of the two lines along which the six 2D imaging profiles are arranged. These profiles, as illustrated in Fig. (10 and 11) reveal four distinct geoelectrical zones based on differences in resistivity values. Dry deposits of fine sand, gravel, and silt comprise the arid deposits with resistivity values in the early zone, which range from 20 to 600 Ohm.m. Within a range of 4 to 33 meters in thickness, this layer exists. The second zone has resistivity values ranging from 10 to 20 ohm.m, indicating that it is brackish water consisting of coarse sand gravels interspersed with silt. This stratum varies in thickness from 4 to 14 metres. Coarse sand gravels intercalated with silt and clay saturated with saline water comprise the third zone, which has resistivity values ranging from 5 to 10 Ohm.m. Between six and twenty-five meters is the thickness of this zone. Sabkha and clay deposits are classified as the fourth zone, which has a resistivity below 5 Ohm.m. None of the measured profiles in the vicinity of this zone descended to its base. The conclusions drawn from 2D imaging are consistent with the results from VES and well data.

Physiochemical Data

The hydrochemical composition of quaternary groundwater samples collected in the eastern Suez Canal Zone exhibits a notable degree of diversity (Table 3). The observed pH values spanned from 7.1 to 8.8, indicating a marginal inclination towards an alkaline composition. The average electrical conductivity of Quaternary groundwater is 8140 µS/cm, exhibiting a range of 2960 to 15960 µS/cm.

As shown in the TDS distribution map of Quaternary groundwater samples (Fig. 12), there is a significant association between the distance from the coast of the Suez Canal and the TDS values. Seawater intrusion manifests itself conspicuously within a range of less than 3 kilometers. The lateral recharge effect of the irrigation canal becomes apparent at a distance of three to five kilometers. The TDS map of the Quaternary groundwater samples reveals that the high TDS values exceeding 5000 mg/l are closer to the Suez Canal, suggesting that seawater intrusion may be the salinization source; on the other hand, the low TDS values below 5000 mg/l are located to the east, potentially due to the influence of lateral recharge from the irrigation canals and the diminishing effect of seawater intrusion.

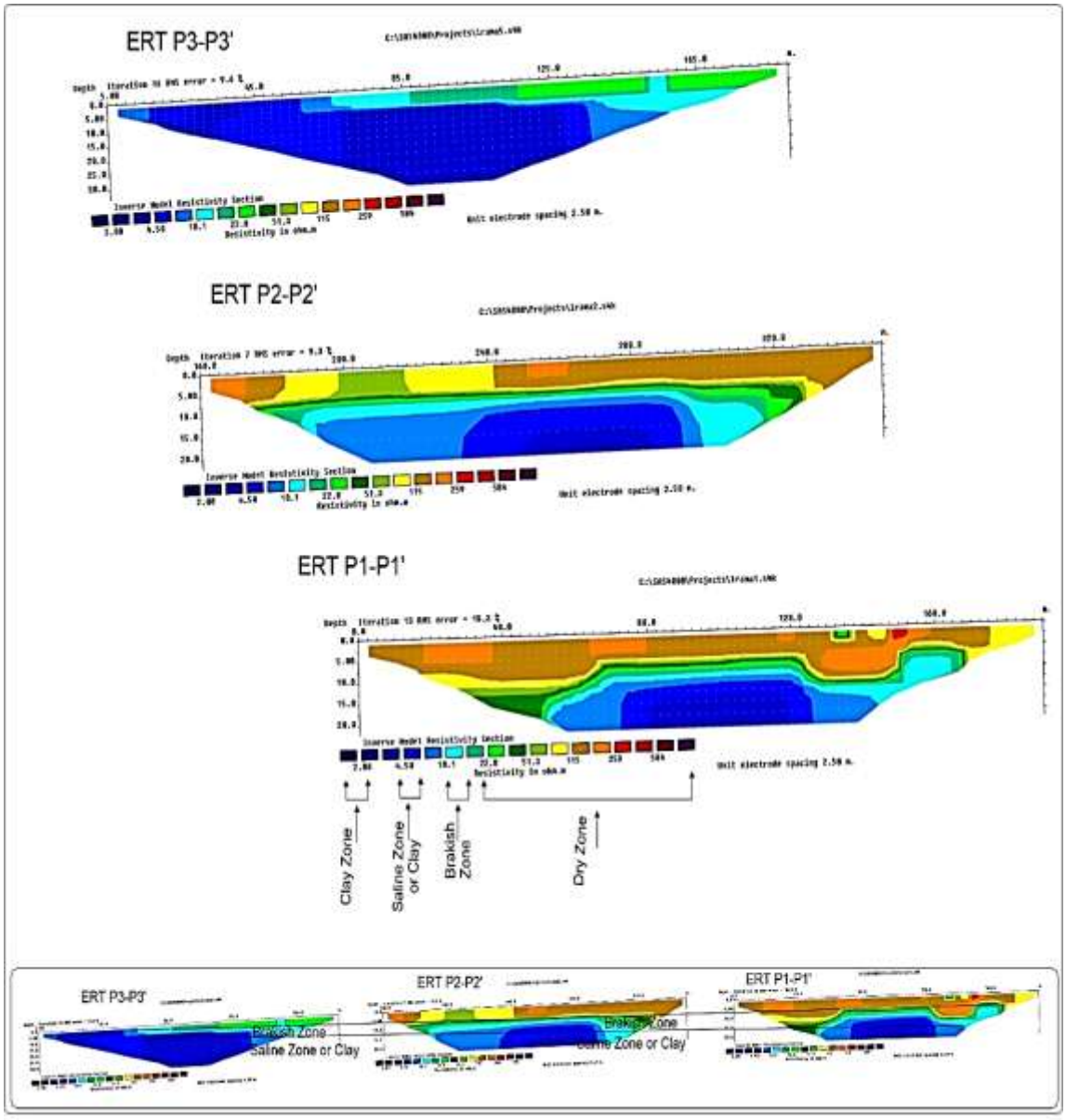

Fig. (10): Illustrates the inversion results of 2D imaging profiles along line 1 in the study, which includes three profiles: 1, 2, and 3.

The dynamics of seawater intrusion were described utilizing the hydrochemical facies evolution diagram (HFED) as proposed by **Gime´nez-Forcada (2010)**. Figure (13) illustrates the location of all groundwater samples in zone No. 4. (Na-Cl facies). Samples Nos. 6, 7, and 15 are located above the incursion line, corresponding to the freshening zone. This is the result of lateral recharge from irrigation canals, which dilutes the fresh water supply. The remaining samples were positioned below the line of intrusion. Most of the groundwater samples taken below the incursion line showed signs that it was either mixing freshwater and saltwater or that marine sediments were dissolving in the aquifer matrix.

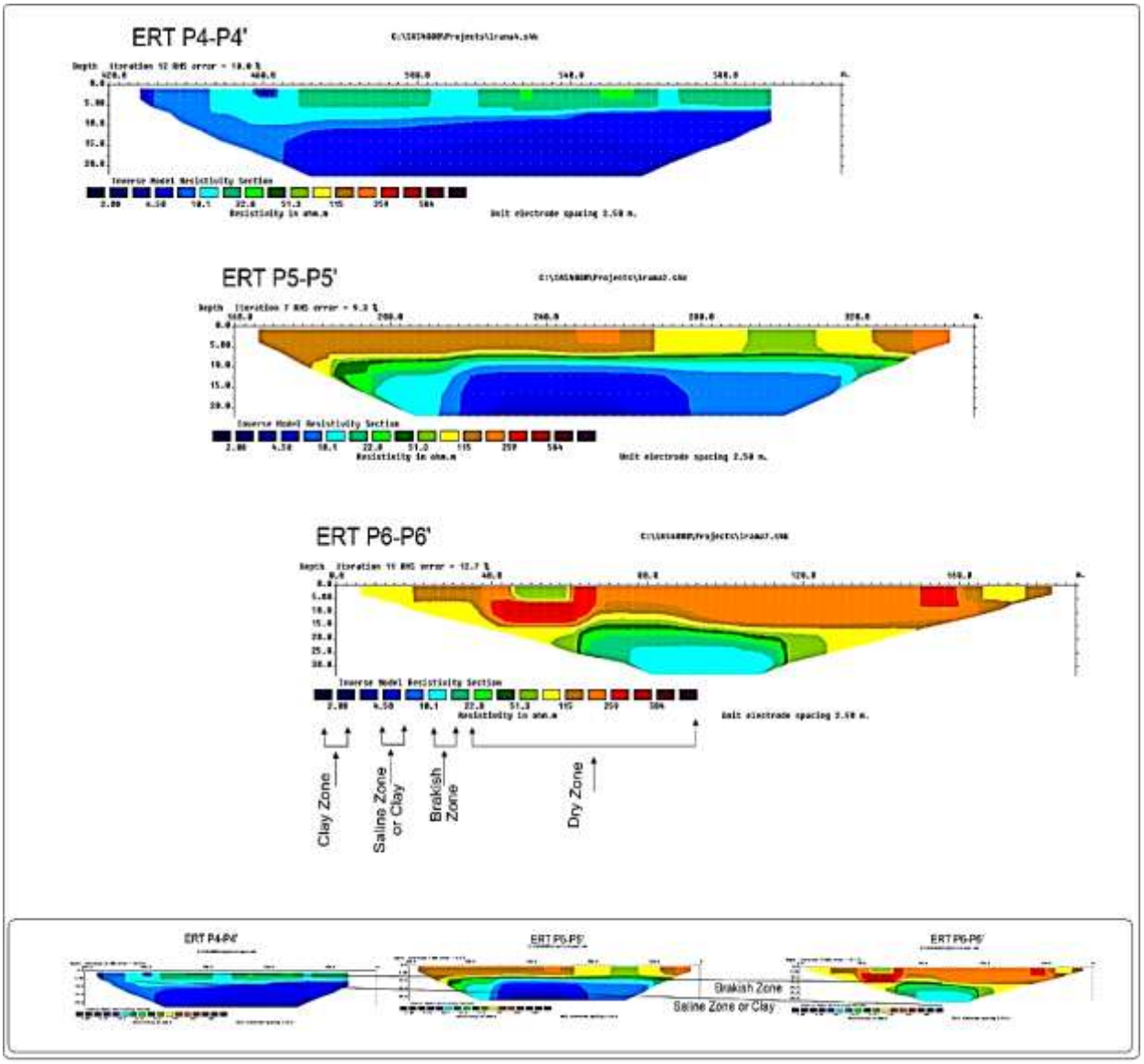

Fig. (11): Illustrates the inversion results of 2D imaging profiles along line 2 in the study, which includes three profiles: 4, 5, and 6.

Intersection of Seawater Mixing

Seawater mixing index (SMI): The cumulative probability curves for the hydrochemical parameters Na^{+}, Mg^{2+}, Cl^{-}, and SO_4^{2-} are graphically shown in Fig. (14). The cumulative probability curves display regional threshold values (T) as inflection points relevant to seawater mixing in the examined region. Approximations were made using the following figures: The concentrations of Na^{+} and Mg^{2+} are 750 mg/l, Cl^{-} is 2612 mg/l, and SO_4^{2-} is 531 mg/l. The regional ion threshold say that the range of sea water mixing values (SMI) is between 0.42 and 2.35T. A study of sample distribution based on SMI values found that SMI levels for groundwater samples collected near the Suez Canal are more than 5,000 mg/l and one as well. This

observation suggests the penetration of saltwater and/or leaching of marine sediments. With SMI values below 1, the TDS values of the groundwater samples in the eastern section of the study region vary from 1765 to 3102 mg/l. Leaching and dissolving processes involving sea sediments exclusively cause salinization of this groundwater. Figure 14 illustrates the cumulative probability curves for the hydrochemical parameters Na^{+}, Mg_2^{+}, Cl^{-}, and SO_4^{2-}. The inflection points on the cumulative probability curves represent the regional threshold values (T) for the samples relevant to seawater mixing in the examined region. The following figures were produced as approximations: 531 mg/l for SO_4^{2-}, 750 mg/l for Na^{+}, 96.8 mg/l for Mg^{2+}, and 2612 mg/l for Cl^{-}. The range of sea water mixing values (SMI), as established by the regional threshold values of ions, is between 0.42 and 2.35 T. The results of the sample distribution study, as assessed by SMI values, indicate that groundwater samples collected in the immediate vicinity of the Suez Canal had TDS levels greater than 5000 mg/l and SMI values greater than one. This discovery suggests that seawater penetration and/or leaching of marine deposits are possibilities. The groundwater samples in the eastern section of the study region have TDS values ranging from 1765 to 3102 mg/l, while the SMI values remain below 1. Leaching and dissolving activities utilizing sea sediments are the sole mechanisms by which this groundwater becomes salinized.

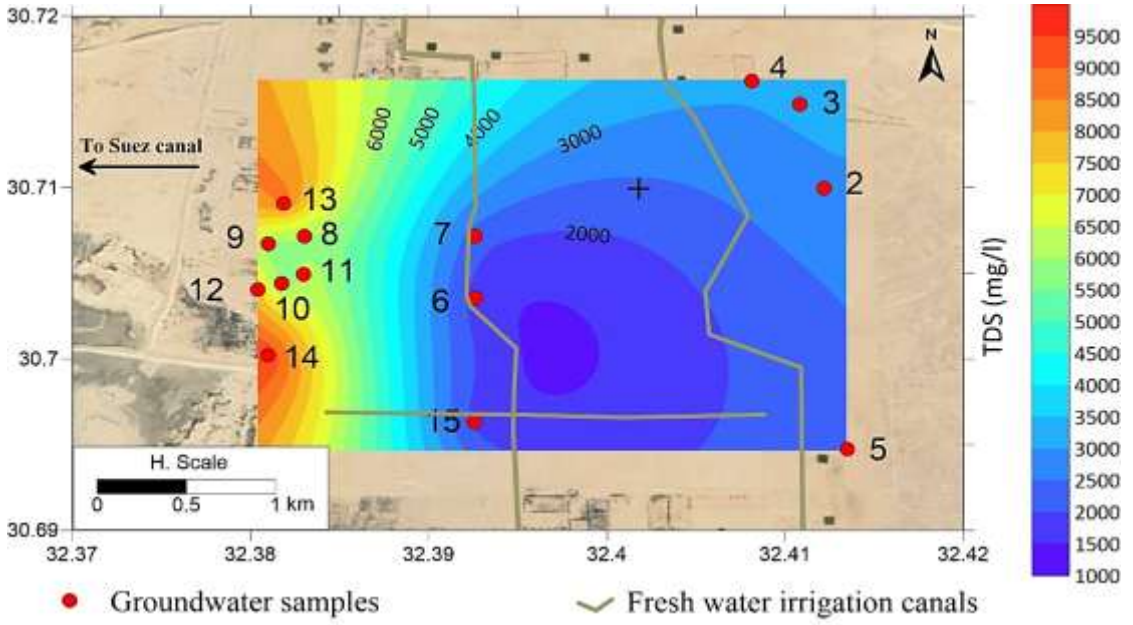

Fig. (12): Distribution of TDS values of Quaternary groundwater.

Table (3): Results of water quality analysis for the area investigated

No	Type	pH	EC	TDS	Ca^{2+}	Mg^{2+}	Na^{+}	K^{+}	CO_3^{2-}	HCO_3^{-}	SO_4^{2-}	Cl^{-}	SMI
			µS/cm	mg/l	mg/l	mg/l	mg/l	mg/l	mg/l	mg/l	mg/l	mg/l	
1	I.C	7.5	341	231.9	27.9	16.9	30	6	9	134.2	25.7	49.3	-
2	G. W	7.2	5120	2927.1	251.0	96.8	675	5	6	76.3	253.2	1602.0	0.71
3	G. W	7.2	5220	3102.0	270.9	82.3	725	6	0	79.3	425.5	1552.7	0.74
4	G. W	7.1	5280	3099.9	257.8	79.1	750	6	0	81.5	408.8	1557.4	0.74
5	G. W	7.3	4460	2499.1	215.1	96.8	575	6	0	94.6	80.2	1478.7	0.61
6	G. W	8.8	2960	1765.4	114.9	63.8	430	5	12	97.6	350.6	740.3	0.42
7	G. W	8.1	3880	2263.3	159.4	67.8	550	5	0	85.4	452.7	985.8	0.54
8	G. W	7.1	10360	5992.8	394.0	164.6	1500	5	0	105.1	471.4	3405.3	1.35
9	G. W	7.1	9450	5769.2	386.5	142.8	1450	5	0	109.8	471.2	3258.9	1.31
10	G. W	7.1	9270	5621.0	350.6	147.6	1650	6	0	100.7	504.0	2912.4	1.54
11	G. W	7.2	11130	6346.1	414.3	164.6	1700	5	0	161.7	531.0	3450.4	1.60
12	G. W	7.1	12590	7696.5	725.1	58.1	2000	6	0	164.7	881.8	3943.3	1.84
13	G. W	8.1	15240	8725.5	737.0	254.1	2100	9	0	79.3	508.8	5077.0	2.16
14	G. W	8.0	15960	9507.5	677.3	242.0	2400	7	0	109.8	1197.3	4929.1	2.35
15	G. W	8.8	3050	1854.6	122.1	65.6	450	5	12	98.6	370.2	780.4	0.44
Suez Canal		8.6	58400	33736.1	371.0	1257.0	9820	610	12	193.5	3219..3	18350.0	-
I.C: Irrigation Canal G.W: Groundwater													

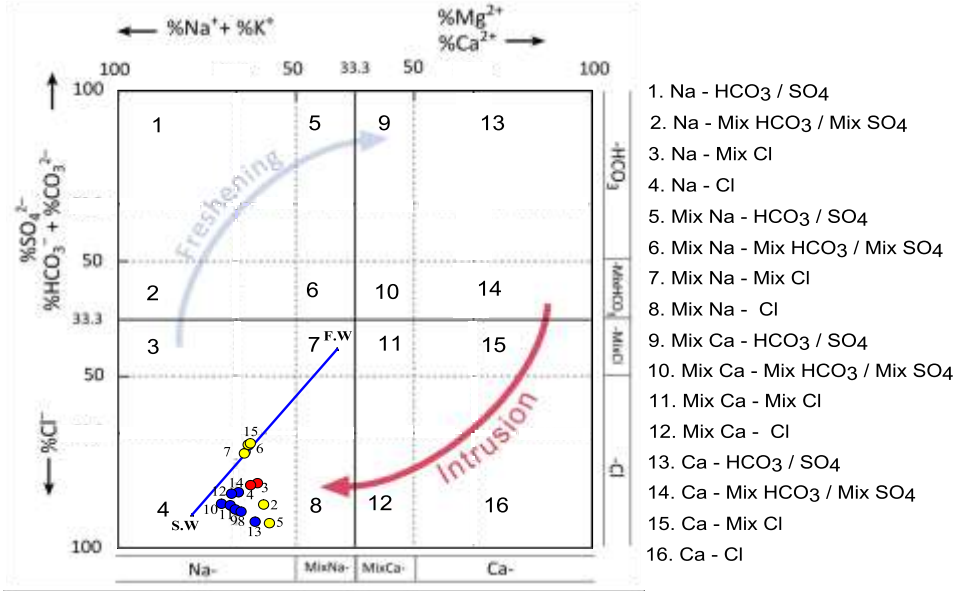

Fig. (13): Hydrochemical Facies Evolution Diagram HFED

Groundwater Quality Index for Seawater Intrusion

The study area showed that groundwater samples close to the shore of the Suez Canal (10-50% of the samples, or GQI_{SWI}<50) are salty because seawater has seeped in. This is shown by the Quaternary groundwater quality index for seawater intrusion in Table (4). The inclusion of seawater has an impact on the aforementioned samples, including Nos. 8, 9, 10, 11, 15 and 14. With a GQI_{SWI} score between 50 and 75, however, half of the groundwater samples demonstrate a blended characteristic (Fig. 15).

Table (4): Results of Groundwater Quality Index for Seawater Intrusion (GQISWI) for the quaternary groundwater samples in the study area.

No.	$GQI_{Piper\ mix}$	GQI_{fsea}	GQI_{SWI}	No.	$GQI_{Piper\ mix}$	GQI_{fsea}	GQI_{SWI}
2	21.7	91.5	56.6	9	17.3	82.5	49.9
3	20.7	91.8	56.3	10	15.5	84.4	49.9
4	19.8	91.8	55.8	11	17.0	81.4	49.2
5	23.0	92.2	57.6	12	17.0	78.7	47.9
6	21.1	96.2	58.6	13	19.7	72.5	46.1
7	19.8	94.9	57.3	14	17.5	73.3	45.4
8	17.6	81.7	49.7	15	21.0	96.0	58.5

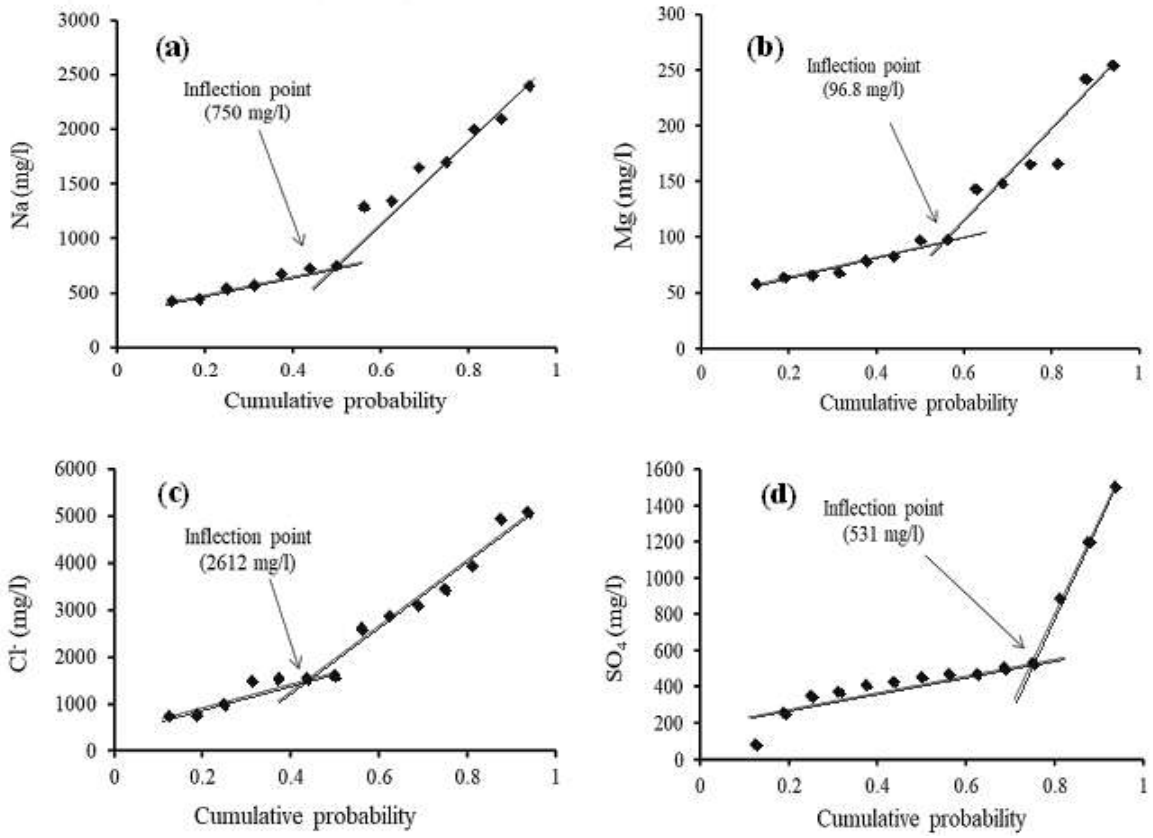

Fig. (14): The cumulative probability curves for the estimation of inflection points (regional threshold values) for Na, Mg, Cl, and SO_4 based on Sinclair (1974)

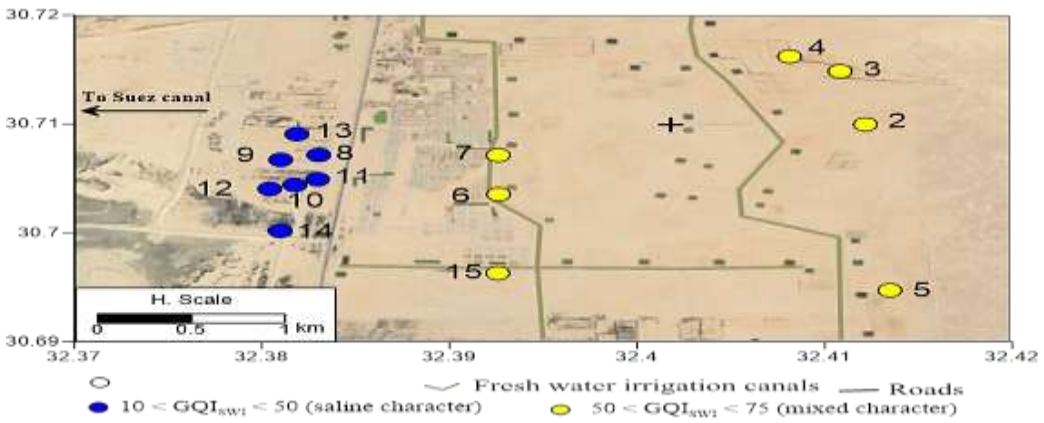

Fig. (15): Groundwater classification map according to GQISWI

Conclusions

Based on the conclusions of the current investigation, there are four geoelectrical layers (A, B, C, and D). Two of them (B and C) represent the waterbearing layers; layer B represents brackish waterbearing sand and gravel, while layer C represents saline waterbearing fine sand and gravels intercalated with silt and clay. The existing visibility of the brackish water in the B layer along the area is weak to moderate because of the existence of a brackish-saline water interface. The interface's depth increased toward the east, ranging from 5 to 70 m from the earth's surface. The results of the Quaternary groundwater samples show a significant correlation between the distance from the Suez Canal coast and the hydrochemical composition. The seawater intrusion effect has clearly appeared near the Suez Canal at a distance of less than 3 km. The lateral recharge of the irrigation canal has an effect at a distance of 3 to 5 km. According to the hydrochemical facies evolution diagram (HFED), all of the groundwater samples are in the Na-Cl facies zone because of seawater intrusion. Some samples (Nos. 6, 7, and 15) are located above the intrusion line (freshening zone) due to dilution by the freshwater source through the lateral recharge from irrigation canals. The remaining samples were located below the intrusion line. Most of the groundwater samples located below the intrusion line reflected the mixing between seawater and freshwater and/or the dissolution of marine deposits in the aquifer matrix. The Quaternary groundwater quality index indicates that groundwater samples in the research area, which are in close proximity to the Suez Canal coast, have a saline nature as a result of seawater intrusion. However, 50% of the groundwater samples show mixed character. The integration of the geophysical and hydrochemical results recommends the eastern part of the study region for new wells, with a maximum depth of 76 m, and the western part for hand-dug wells with a maximum depth of 8 m. The design must depend on the thickness of the layer B. The pumping test is critical in determining the savings yield for future wells.

Statements and Declarations

Data availability: This manuscript has no associated data.

Competing interests: The authors report there are no competing interests to declare.

Funding: This research received no external funding.

Acknowledgments: The author expresses gratitude to the Geophysics Department and hydrogeochemistry laboratory of the Desert Research Center (DRC), Cairo, Egypt, for their assistance.

References

Abdel Hafeez, T., Sabet, H., El-Sayed, A., Zayed, M., (2018). Geoelectrical exploration of groundwater at West Dayrout Area, Assiut Governorate, Egypt. *NRIAG J. Astronomy Geophys.*, 7(2): 279-296.

Al-Mahemmdi, W., Al-Baana, A., Al-Menshed, F., (2023). An integrated microgravity and soil analysis methods to assist the resistivity profiles interpretation in an engineering site southern Baghdad, Iraq. *Iraqi Geol. J.*, 56 (2F): 265-275 .

Appelo, A., Postma, D., (2005). Geochemistry, groundwater and pollution. 2nd, pp. 17. Rotterdam: Balkama.

ASTM (American Society for Testing and Materials) (2002). Water and Environmental technology". Annual book of ASTM. Standards, U.S.A. Sec. 11, Vol. 11.01, and 11.02, West Conshohocken.

Barer, S., Mhli, S., Singh, A., Arora, C., Gil, K., (2000). Sewer water irrigation effects on some potentially toxic trace elements in soil and potato plants in northwestern India". *Cand. J. Soil, Sci.* 185 .

Barker R.D., (1980). Application of Geophysics in groundwater investigations. *Water Surv*., 84: 489-492.

Bear, J., (1999). Conceptual and mathematical modeling in Seawater intrusion in coastal aquifers. Springer, Netherlands, pp. 127-161.

Boluda-Botella N., Valdes-Abellan J., Pedraza R., (2014). Applying reactive models to column experiments to assess the hydrogeochemistry of seawater intrusion: optimising ACUAINTRUSION and selecting cation exchange coefficients with PHREEQC. *J Hydrol* ., 510:59-69.

Brown, E., Skougstad, M. W., Fishmen, M. J., (1983). Method for collection and analyzing of water samples for dissolved minerals and gases (p. 75). Washington DC, USA: U.S. Govt. Printing Office.

Clement, R., Fargier, Y., Dubois, V., Gance, J., Gros, E., Forquet, N., (2020). OhmPi: An open-source data logger for dedicated applications of electrical resistivity imaging at the small and laboratory scale. HardwareX, 8, e00122.

Diab, F., (1998). Geology, pedology and hydrogeology of the Quaternary deposits in Sahl El Tinah area and its vicinities for future development of north Sinai, Egypt. Ph. D. Thesis, Fac. of Sci. Mansoura Univ. Egypt, 242.

El Abd, E. A., (2000). Contribution to the hydrogeology of Northwest Sinai, Egypt. M. Sc. Thesis, Fac. Sci., Minufiya Univ., Egypt, 165p.

Elewa, H., Qaddah, A., (2011). Groundwater potentiality mapping in the Sinai Peninsula, Egypt, using remote sensing and GIS-watershed-based modeling. *Hydrogeol. J.*, 19: 613– 628.

Frohlich, R. K., Urish, D. W., Fuller, J., O'Reilly, M., (1994). Use of geoelectrical methods in groundwater pollution surveys in a coastal environment. *J. appl. Geophys*., 32(2-3): 139-154.

Gibbs M.S., Dandy G.C., Maier H.R., (2013). Assessment of the ability to meet environmental water requirements in the Upper Southeast of South Australia. *Stoch. Env. Res. Risk Assess*.

Gime´nez-Forcada E., (2010). Dynamic of seawater interface using hydrochemical

facies evolution diagram. Ground Water, 48 (2): 212-216.

Griffiths, D. H., Barker, R. D., (1993). Two-dimensional resistivity imaging and modelling in areas of complex geology. *J. appl. Geophy*., 29(3-4): 211-226.

Hassan, M., Shang, Y., Akhter, G., Jin, W., (2019). Application of VES and ERT for delineation of fresh-saline interface of lower Bari Doab, Pakistan, *J. Appl. Geophy*., 164: 200-213.

Kouzana, L., Benassi, R., Ben Mammou, A., Sfar Felfoul, M., (2010). Geophysical and hydrochemical study of the seawater intrusion in Mediterranean semiarid zones, case of the Korba coastal aquifer (Cap-Bon, Tunisia). *J. Afr. Earth Sci.*, 58(2): 242-254 .

Kusumayudha, S. B., Zakaria, M. F., Setyaningrum, T., (2023). Geological Factor Causing Water Decrease of the Baturagung Reservoir, Based on ERT Geoelectric Application. *Iraqi Geol. J.*, 56(1D): 103-113.

Loke M.H., (1999). Electrical imaging surveys for environmental and engineering studies. Cangkat Minden Lorong. 6574525:57.

Mondal, N. C., Singh, V. P., (2011). Hydrochemical analysis of salinization for a tannery belt in Southern India. *J. Hydrol.*, 405(3-4): 235-247.

Najib, S., Fadili, A., Mehdi, K., Riss, J., Makan, A., (2017). Contribution of hydrochemical and geoelectrical approaches to investigate salinization process and seawater intrusion in the coastal aquifers of Chaouia, Morocco. *J. Contam. Hydrol.*, 198: 24-36.

Panteleit B., Hamer K., Kringel R., Kessels W., Schulz H. D., (2011). Geochemical processes in the saltwater-freshwater transition zone: comparing results of a sand tank experiment with field data. *Env. Earth Sci*., 62: 77-91.

Park, S.C., Yun, S.T., Chae, G.T., Yoo, I.S., Shin, K.S., Heo, C.H., Lee, S.K., (2005). Regional hydrochemical study on salinization of coastal aquifers, western coastal area of South Korea. *J. Hydrol.*, 313(3-4): 182-194.

Qahman K., Larabi A., Ouazar D., Naji A., Alexander H., Cheng D., (2005). Optimal and sustainable extraction of groundwater in coastal aquifers. Stochastic Environmental Research and Risk Assessment. 19:99-110

Qudsiah, R. A., Al-Amoush, H. R., Al Adamat, R. A., (2024). Groundwater Recharge Potential Assessment in Azraq Basin, Jordan Using Multi-Criteria Decision Making (MCDM)-GIS and Geophysical Techniques. The *Iraqi Geol. J.*, 287-307.

Sinclair, A.J., (1974). Selection of thresholds in geochemical data using probability graphs. *J. Geochem. Explor.* 3: 129-149.

Sultan, A., Hatem M. M., Fernando M. S., (2009). Groundwater exploration and evaluation by using geophysical interpretation (case study: Al Qantara East, Northwestern Sinai, Egypt). Arab J Geosci 2:199-211.

Tomaszkiewicz, M., Abou Najm, M., El-Fadel, M., (2014). Development of a groundwater quality index for seawater intrusion in coastal aquifers. Environmental Modelling & Software, 57: 13-26.

Zayed, M., Nasr, A., (2023). Detection of Fractured Limestone Landslides Using Electrical Resistivity Tomography: A Case Study in the Mokattam Plateau, Egypt. *Iraqi Geol. J.*, 56 (2C): 143-152.

دراسة تأثير تداخل المياه المالحة على الخزان الجوفى الرباعى باستخدام الطرق الجيوفيزيائية بمدينة الأمل، شرق الاسماعيلية، مصر

أحمد نصر
مركز بحوث الصحراء، قسم الاستكشاف الجيوفيزيائى، القاهرة، مصر

تهدف هذه الدراسة إلى تحديد النطاقات الأفقية والرأسية للمياه متوسطة الملوحه داخل طبقة المياه الجوفية الرباعية في منطقة غنية بالموارد باستخدام مزيج من الطرق الهيدروكيميائية والجيوفيزيائية. تم تحليل أربع عشرة عينة من المياه الجوفية وعينتين من المياه السطحية لتحديد الأنيونات والكاتيونات الرئيسية لتقييم جودة المياه وتداخل المياه المالحة. تم حساب مؤشر خلط مياه البحر، بناءً على تركيزات أيونات المغنيسيوم والصوديوم والكبريتات والكلوريد، لتقدير تداخل مياه البحر. بالإضافة إلى ذلك، تم تطوير مؤشر لجودة المياه الجوفية لقياس درجة تداخل مياه البحر. تم إجراء ستة عشر قياسًا كهربائيًا عموديًا من نوع شلمبرجير وعشرة قطاعات ثنائية الأبعاد على طول خطين، مما كشف عن أربع طبقات جيوكهربية: رمل ناعم وطين جاف، رمل وطين يحملان مياه متوسطة الملوحه، رمل وطين يحملان مياه مالحه، وطبقة من الطين. تشير النتائج إلى أن المياه الجوفية بالقرب من قناة السويس تظهر علامات على تداخل المياه المالحة. ومع ذلك، تشير ٥٠% من العينات أيضًا إلى ذوبان الرواسب البحرية أو المياه العذبة. توصي الدراسة بحفر آبار جديدة بعمق يصل إلى ٧٦ مترًا في الجزء الشرقي من المنطقة، بينما الآبار المحفورة يدويًا مناسبة للمنطقة الغربية بعمق ٨ أمتار.